J Ther Eng, Vol. 9, No. 5, pp. 1291−1306, September, 2023

Journal of Thermal Engineering
Web page info: https://jten.yildiz.edu.tr
DOI: 10.18186/thermal.1376850

Journal of Thermal Engineering

Research Article

Effect of heat flux and mass flux on the heat transfer characteristics of supercritical carbon dioxide for a vertically downward flow using computational fluid dynamics and artificial neural networks

Rajendra PRASAD K S[1,*], V KRISHNA[2], Sachin BHARADWAJ[2]

[1]*Department of Mechanical Engineering, Manipal Institute of Technology, Bangalore, 560064, India*
[2]*Department of Mechanical Engineering at PES University, Bangalore, 560064, India*

ARTICLE INFO

Article history
Received: 05 March 2022
Revised: 04 July 2022
Accepted: 12 July 2022

Keywords:
sCO_2; Vertical Flow; Turbulence Model; CFD; ANN

ABSTRACT

Drastic variation in the thermodynamic properties of supercritical fluids near the pseudo critical point hinders the use of commercial computational fluid dynamics (CFD) software. However, with the increase in computational abilities, along with the use of Artificial Neural Networks (ANN), turbulence heat transfer characteristics of supercritical fluids can be very accurately predicted. In the present work, heat transfer characteristics for a vertically downward flow of carbon dioxide in a pipe are studied for a wide range of heat flux and mass flux values. Firstly, six different turbulent models available in the commercial CFD software - Ansys Fluent are validated against the experimental results. The k- ω Standard model with enhanced wall treatment is found to be the best-suited turbulence model. When experimental results were validated in CFD, an average error of 1% in the bulk fluid temperature and 2% in the wall temperature were recorded. Further, K- ω Standard Turbulence Model is used in CFD for parametric analysis to generate the data for ANN studies. Mass flux range of 238 to 1038 kg/m^{2}s, and heat flux range of 26 kW/m^2 to 250 kW/m^2 are used to generate 81,432 data samples. These samples were fed into the ANN program to develop an equation that can predict the heat transfer coefficient. It was found that ANN can predict the heat transfer coefficient for the considered range of values within the absolute average relative deviation of 2.183 %.

Cite this article as: Prasad KS R, Krishna V, Bharadwaj S. Effect of heat flux and mass flux on the heat transfer characteristics of supercritical carbon dioxide for a vertically downward flow usingcomputationalfluiddynamicsandartificialneuralnetworks.JTherEng2023;9(5):1291−1306.

INTRODUCTION

The highest temperature and pressure at which vapour and liquid coexist in equilibrium is termed a critical point. Fluids above the critical point exhibit peculiar property variations that can be used to improve heat transfer in fluids, in addition to this, Super Critical Carbon Dioxide (sCO_2) as a working fluid, reduces work input at the inlet to the main compressor, due to its liquid-like behaviour [1]. Nusselt Number correlations applicable to super critical fluids finds lot of application in designing such systems.

*Corresponding author.
*E-mail address: layth.ismael@ozu.edu.tr, 130006@uotechnology.edu.iq

This paper was recommended for publication in revised form by Regional Editor Ahmet Selim Dalkılıç

Water, helium and carbon dioxide are widely used in supercritical heat transfer applications. Carbon dioxide as the working fluid has advantages over other supercritical fluids in terms of lower critical temperature (31.04°C), higher thermal stability and abundant availability. Understanding the heat transfer characteristics of supercritical carbon dioxide near the critical point is very crucial in designing the heat exchangers.

Hall [2] has done extensive work on heat transfer behaviours near a critical point. In this work, Experimental results for forced convection, natural convection and mixed convection were presented along with theoretical methods and correlations for the Nusselt number. Heat transfer enhancement and deterioration were showcased for the forced convection cases. Tanaka et al. [3] have proposed normal mode turbulent convection theory to obtain the wall temperature profiles for forced convection heat transfer to fluids (liquids and gases) near critical point flowing in a circular tube. Higher heat flux values were considered for the study for which surface roughness had a significant effect on forced convection heat transfer to supercritical fluids. Turbulent heat transfer characteristics for supercritical carbon dioxide flow in a pipe of diameter 0.228mm are studied by Bourke et al. [4], this study considered a mass flow rates in the range of 0.127 kg/s to 0.697 kg/s, heat flux range of 8 kW/m^2 to 350 kW/m^2 and a pressure range of 7.4 MPa to 10.32 MPa. These studies have shown, peaks in wall temperature specific to vertical upward flow and these peaks are not observed in vertical downward flows. The authors have also proposed new data for the enthalpy /temperature relationship for carbon dioxide from 15 to 40°C for the above-mentioned operating values.

Fang [5] has given a complete survey of a single phase in tube heat transfer relationships for supercritical carbon dioxide flows. This study highlights the need for new models to understand the heat transfer behaviour near the critical point. Duffey and Pioro [6] have conducted an extensive survey on experimental heat transfer studies for supercritical carbon dioxide flowing inside channels. This study mentions the data regarding the range of operating conditions (Heat flux, mass flux and operating pressure) the researchers have considered for the study over the years. This study concludes that the heat transfer behaviour at supercritical pressures is affected by flow orientations and the operating conditions. Also, the deteriorated heat transfer typically appears at higher heat fluxes and lesser mass flux values regardless of the flow orientations.

Jiang et al. [7] have proposed a technique for obtaining the local heat transfer coefficient of carbon dioxide in a vertically small tube under cooling conditions. Their numerically predicted values of heat transfer coefficient agreed well within 10% error with experimental results. These results were obtained for the mass flux range of 0.5 to 2.2 kg/h, pressure range of 7.4 MPa to 9.5 MPa and a heat flux range of 2.5 to 40 kW/m^2. In this paper, the authors have reported peaks in heat transfer coefficient values for the cases considered near the pseudo critical pressure. These drastic variations in the heat transfer coefficient led to inaccurate predictions if the operating conditions are not within the considered range by the authors. Bae et al. [8] emphasised the need for separate correlations for normal and deteriorated heat transfer regimes. For the 6.32mm pipe diameter and the considered operating ranges (mass flux- 285 to 1200 kg/m^2 s, heat flux – 30 to 170 kW/m^2, operating pressure- 7.75 to 8.12 MPa) the proposed correlation predicted the Nusselt number values within the ±30% deviation. Also, the authors have reported a slight drop in Nusselt number values for vertically downward flow when the buoyancy parameter is in the range of 10^{-7} to $3*10^{-5}$.

Zhang et al. [9] used numerical methods to identify the best-suited turbulence model for the prediction of heat transfer behaviour in supercritical fluids. Reynolds stress models have given a better agreement with the various experimental results considered for the study. The average error using Reynold's stress model is reported at 10.23 % for a q/G value of 0.23 and 9.11% for a q/G value of 0.155. Fang and Xu [10] by considering the 341 experimental data points from various experimental works have proposed a correlation whose relative deviation is 8.9 % which is 14.6% lower than the best existing correlations. Ye et al. [11] have used artificial neural networks (ANN) to develop a correlation to predict heat transfer coefficient (h), with an absolute percentage error of 0.97%, but neglecting the significant effects of buoyancy and flow acceleration in their model, restricts the applicability of the proposed model in buoyancy-driven flows. Wang et al. [12] conducted parametric studies on sCO_2 at low mass fluxes and at high heat fluxes in a horizontal tube where the mass flux ranges from 400-500 kg/m^2 s and heat flux ranges from 30-200 kW/m^2. The studies highlight the main reason for heat transfer deterioration as the buoyancy difference between the top wall and bottom wall. Further studies have shown that the heat transfer coefficient is different for the upper wall and bottom wall, in a horizontal tube. The authors have compared the results with the correlation proposed by Liao – Zhao [13] and the results agree well with their experimental data. Recently, Rajendra Prasad et al. [14] used Artificial Neural networks for deriving the generalized correlations for Nusselt Number for supercritical carbon dioxide flowing upwards in a pipe, where the average deviation is less than 10%.

Though many correlations are available in the literature to predict 'Nusselt Number', using numerical approach for supercritical-fluids-pipe-flow, the relative deviation of results such equations is more than 10% compared to the experimental results. Further, the applicability of these correlations is also limited to a narrow range of operating parameters.

In the present work, firstly CFD methodology adopted is validated against the existing experimental studies [16]. Later, using the validated CFD methods, a wide range of parametric studies with varying - heat flux and mass flux is carried out. A total of 81,432 data samples obtained from

18 different operating conditions are used to train ANN, which resulted in a more generalized correlation for a downward flow of supercritical carbon dioxide at the operating pressure of 7.631 MPa. This equation with the given weights and bias can predict the heat transfer coefficient for the whole range of operating conditions within 2.183 % of average absolute relative deviation.

METHODOLOGY

Geometric Modelling

Ansys Design modeler is used to create a vertical pipe with an inner diameter of 2 mm, the outer diameter of 3.137 mm and a length of 290 mm as shown in Figure 1. The length and diameters of the pipe are grounded in the experimental works of Li et al. [16]. The inner wall of the solid domain is coupled to the outer surface of the fluid domain to establish a connection between solid and fluid domains.

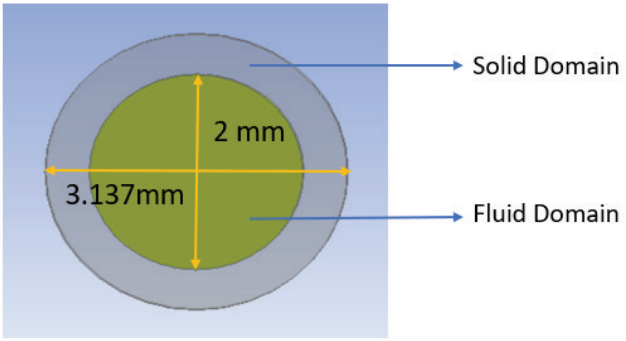

Figure 1. Geometry (Top View).

Mathematical Modelling

Conservation equations

Numerical solutions rely on the three fundamental fluid flow equations namely, conservation of mass, momentum and energy. Equations 1, 2, and 3 represent averaged forms of these equations in index form. Steady flow equations are used in the present work.

$$\frac{\partial \overline{u_i}}{\partial x_i} = 0 \tag{1}$$

$$\left(\rho \frac{\partial \overline{u_i}}{\partial t} + \overline{u_j} \frac{\partial \overline{u_i}}{\partial x_j}\right) = -\frac{\partial \overline{p}}{\partial x_i} + \frac{\partial \overline{\tau_{ij}}}{\partial x_j} - \frac{\partial}{\partial x_j}\left(\overline{\rho u'_i u'_i}\right) \tag{2}$$

Here τ_{ij} is the laminar shear stress tensor is given by $\overline{\tau_{ij}} = \mu\left(\frac{\partial \overline{u_i}}{\partial x_j} + \frac{\partial \overline{u_j}}{\partial x_i}\right)$

and the Reynolds stress is given by $\overline{\rho u'_i u'_i} = -\mu_T\left(\frac{\partial \overline{u_i}}{\partial x_i} + \frac{\partial \overline{u_j}}{\partial x_i}\right)$

$$\frac{\partial}{\partial x_j}\left(\overline{u_j} \cdot \overline{T}\right) = \frac{\partial}{\partial x_j}\left(\alpha \frac{\partial \overline{T}}{\partial x_j} - \overline{u'_j \cdot T'}\right) \tag{3}$$

here α is the thermal diffusivity $\alpha = \frac{K}{\rho C_p}$, where K is the thermal conductivity in W/m-K

Turbulent heat diffusion may be approximated as $\overline{u'_j \cdot T'} = -\alpha_T \frac{\partial \overline{T}}{\partial x_j}$

ANSYS Fluent has several turbulence models inbuilt to solve Reynold's stress components. The k-ε std, k-ε Realizable, k-ε RNG, k-ω Std, k-ω BSL and k-ω SST models are the more popular turbulence models used in the previously available literature.

Computational Fluid Dynamics (CFD) Modelling

Heat transfer characteristics of supercritical fluids are very different from that of normal fluids [5]. Numerical methods with the appropriate boundary conditions and solution algorithms, prove to be very effective in predicting heat transfer characteristics of supercritical fluids. In the present work, to evaluate the accuracy of turbulent models available in the software, six different models namely k-ε std, k-ε Realizable, k-ε RNG, k-ε Std, k-ω BSL and k-ω SST were chosen. A total of six simulations were performed as part of the validation.

Properties of supercritical fluids vary drastically near the critical point. These property variations can be incorporated into the ANSYS FLUENT by establishing an interface between FLUENT and NIST REFPROP [12] database. Stainless steel 316L properties are used for the solid domain. The coupled scheme is used for Pressure-velocity equations. density, momentum, turbulent kinetic energy terms, turbulent dissipation rate and energy terms are solved using third-order spatial discretization. Body force weighted scheme for pressure spatial discretization is used to include buoyancy effects.

Calculations are continued until the convergence criteria are achieved as shown in Figure 2 and Figure 3. During the first few iterations, the convergence parameter (mass outflow – mass inflow) oscillates and as the iterations continue the magnitude of oscillation is reduced and mass conservation is achieved at around 450 iterations for the case shown below. As a second convergence criterion, outlet temperature is monitored during the iterations. Similar to the mass conservation criteria, outlet temperature fluctuates during the first few iterations and once the results tend towards convergence of 10^{-3}, the magnitude of fluctuations is reduced.

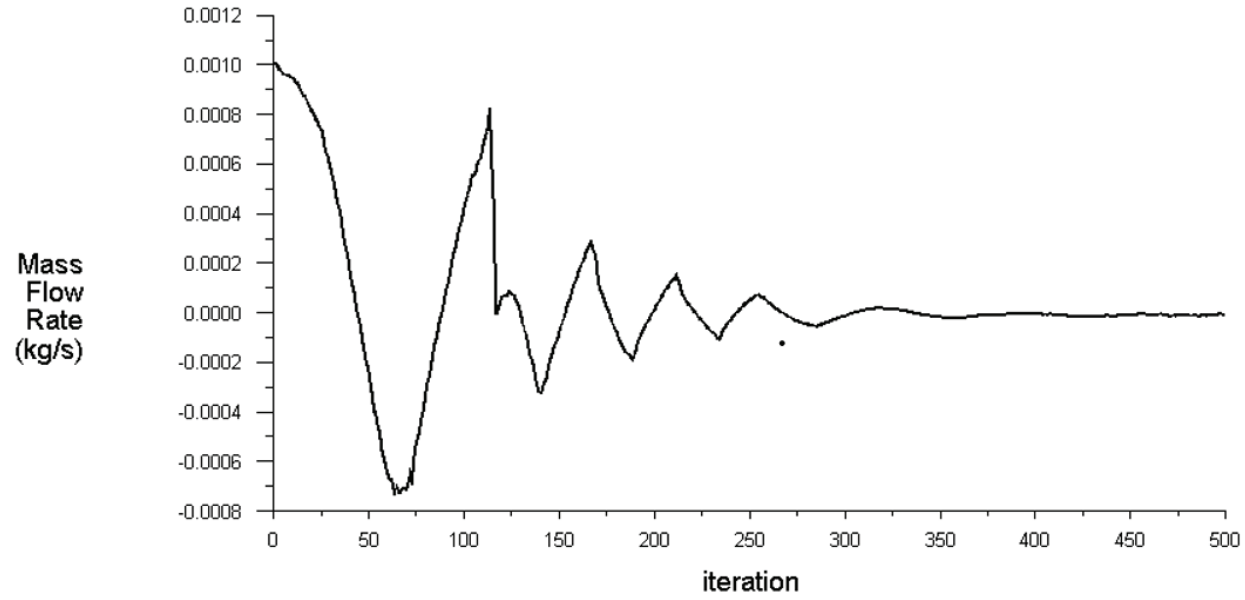

Figures 2. Report definition plot for the difference between mass outflow and mass inflow).

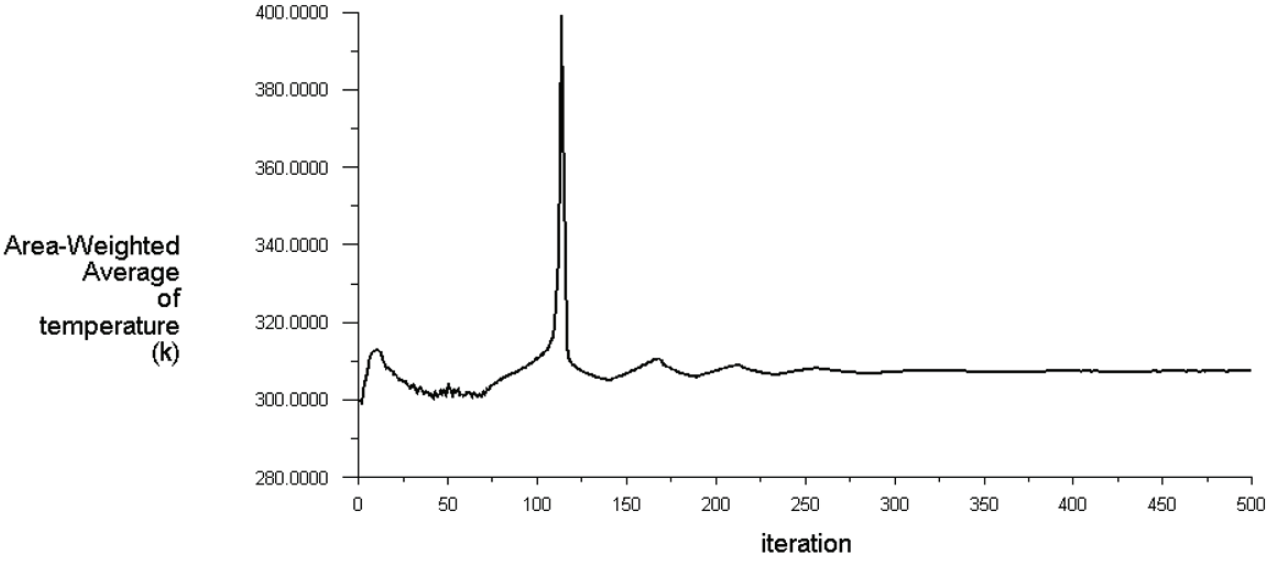

Figures 3. Report definition plot for outlet bulk fluid temperature.

Mesh independence study

Before the detailed parametric studies, a mesh independence study was conducted. Ansys-workbench provides mesh metrics to measure and monitor the quality of the mesh generated. A total of six meshed models are created with the 5 layers of inflation to see the variation of the bulk fluid outlet temperature with the increase in the number of elements. Grid independent results are obtained for 84,70,952 elements (Figure 4b) with an element size of 0.0002m with 5 layers of inflation as shown in Figure 4a. In all the meshed models used in the analysis, target Y^+ of 1 is set to capture the effects of viscous sub-layers. Mesh metric details are mentioned in Table 1. The addition of inflation layers greatly reduced the distance of the first element from the wall. The distance from the wall to the first element in the mesh is 0.000025m. The inflation layers provide accuracy in the final results by capturing small temperature differences as well as drastic property variations between the wall and the fluid.

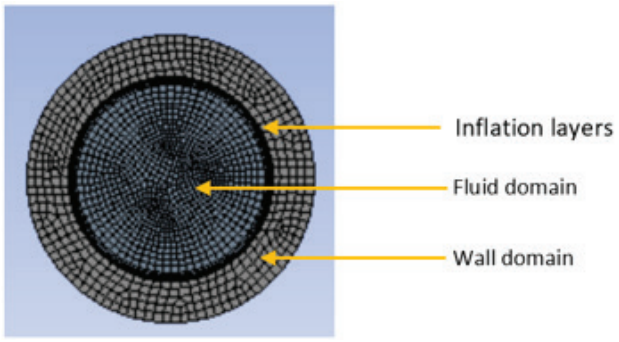

Figure 4a. Meshed model.

Figure 6. In all these cases a target Y^+ of 1 is choosed to compare the different turbulence models. All the turbulence models predicted the bulk fluid temperature within the error percentage of ± 2%, while, the error % in wall temperature prediction of other turbulent models is greater than 2%, except the k-w Std model whose wall temperature prediction is within 1% deviation. Hence the k-w Std model is used for the parametric analysis in this work.

Nusselt number graphs from the experimental results of Li et al. [16] are used to verify the accuracy of the selected

Table 1. Mesh Metrics

Number of Elements	Element Quality (Avg.)	Skewness (Avg.)	Aspect Ratio (Avg.)	Orthogonal Quality (Avg.)
84,70,952	0.7638	0.083	2.3195	0.98588

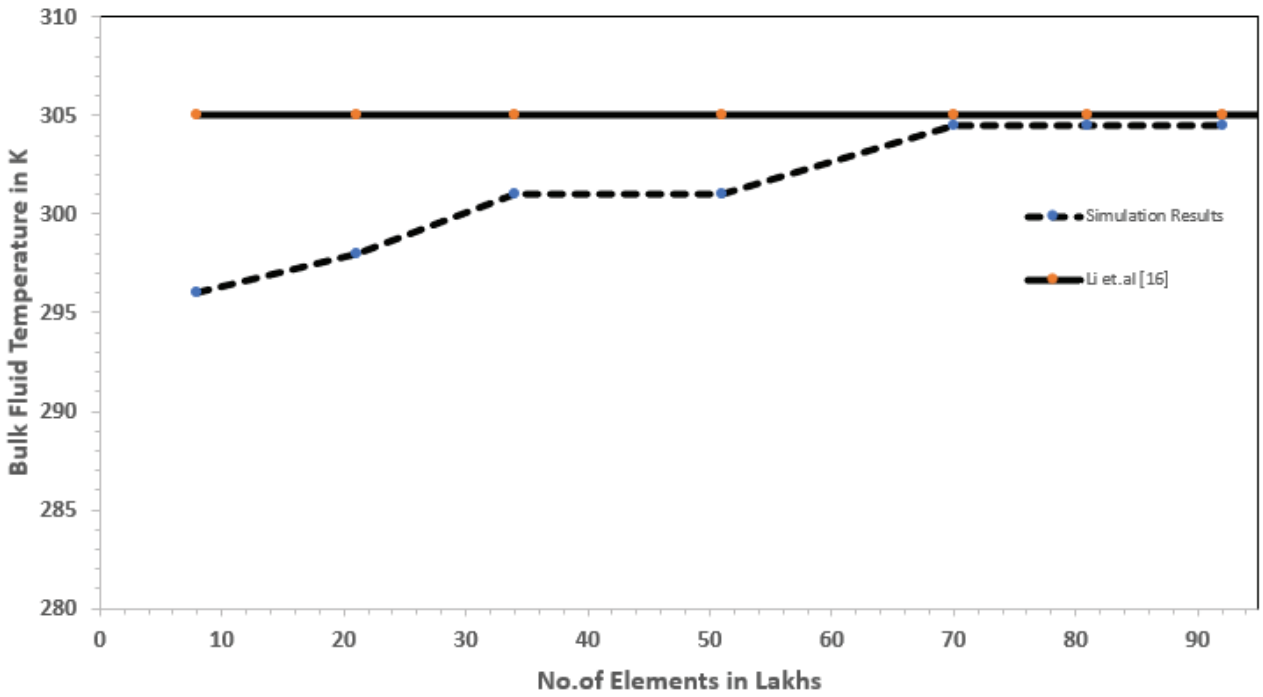

Figure 4b. Number of elements v/s Bulk fluid temperature.

Validation of the Present Study

To evaluate the accuracy of our CFD methods and different turbulence models available in the software, a comparative study is conducted against the experimental results of Li et al. [16]. Seven different turbulence models are used to plot Bulk fluid temperature and inner wall temperatures against the experimental results as shown in Figure 5 and

k-ω std turbulence model. Figure 7, shows the variation of the Nusselt number against the location for different turbulence models. Compared to the other models for which the deviation is more than 150%, the k-ω std model predicted the Values of the Nusselt number with an average deviation of 25%.

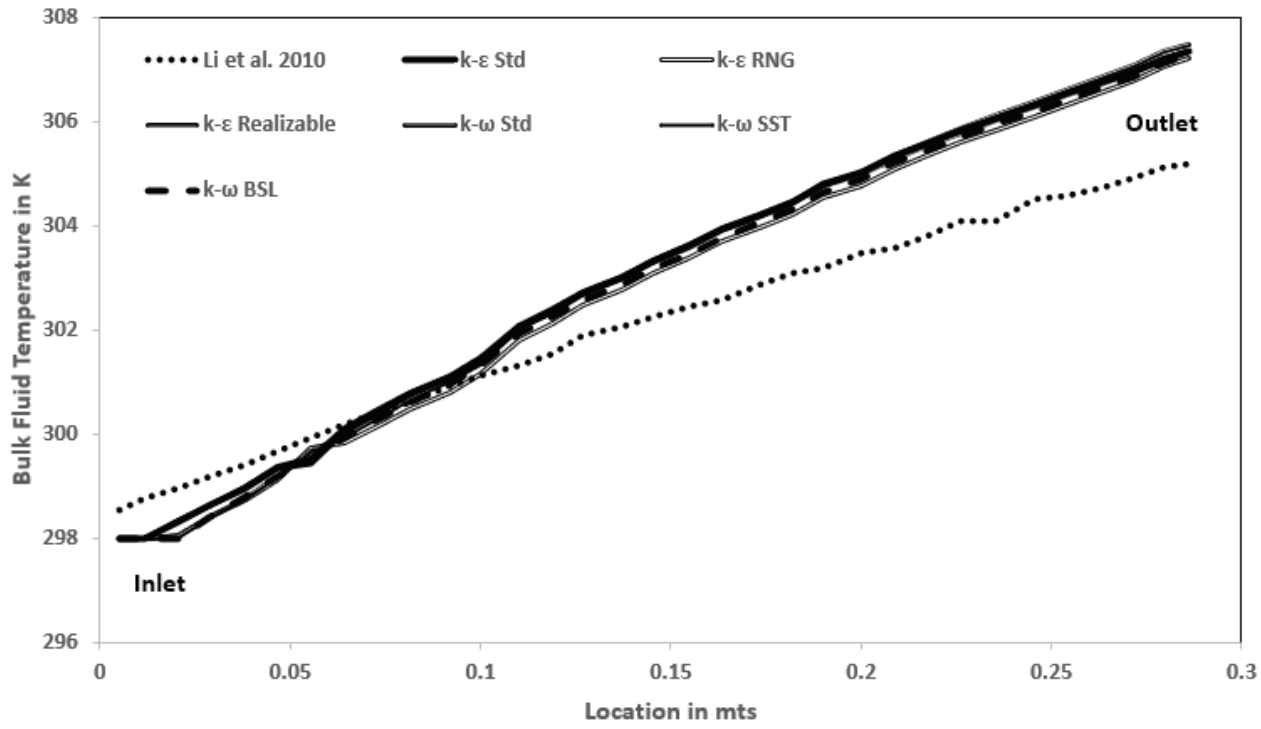

Figure 5. Bulk fluid temperature variation along the pipe length. (Li et al. [11]: Downward Flow, P=8.80 MPa, T_{in} = 25^{0}C, Re_{in} = 9000.)

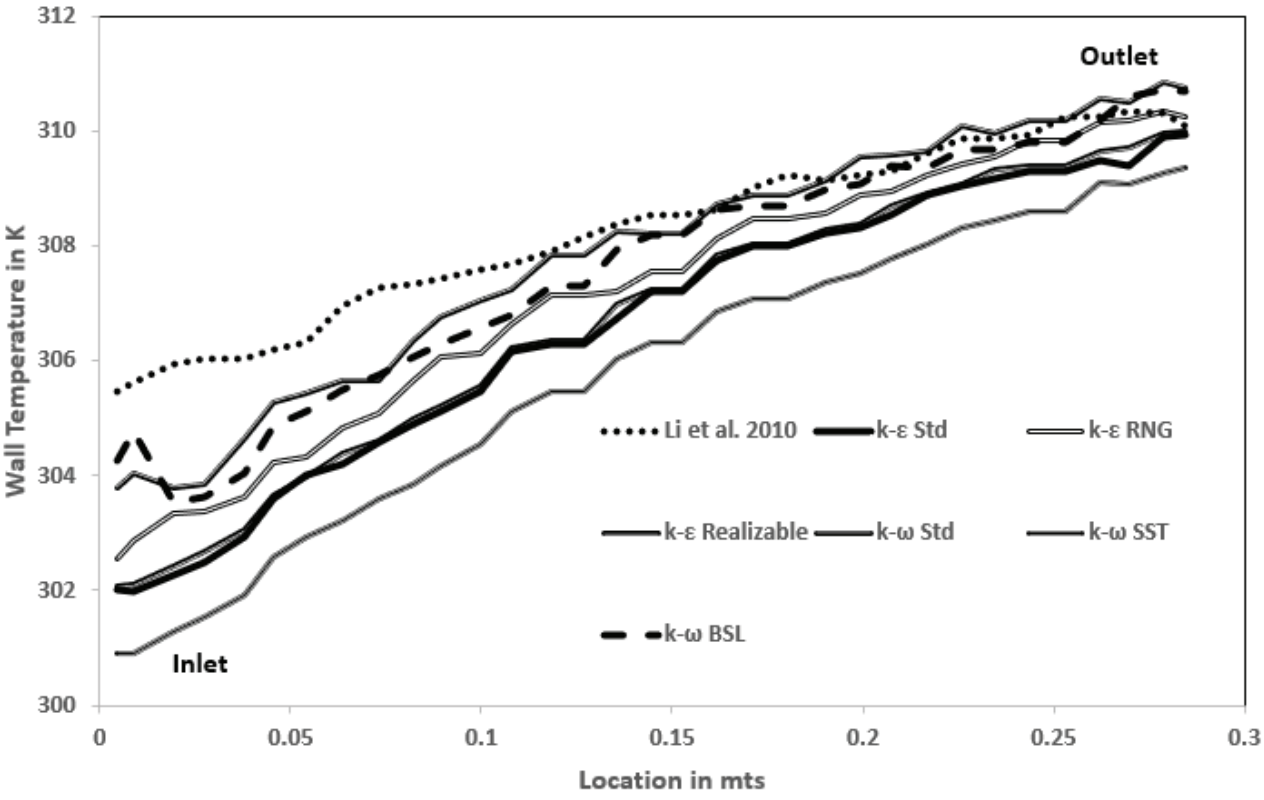

Figure 6. Wall temperature variation along the pipe length. (Li et al. [11]: Downward Flow, P=8.80 MPa, T_{in} = 25^{0}C, Re_{in} = 9000.)

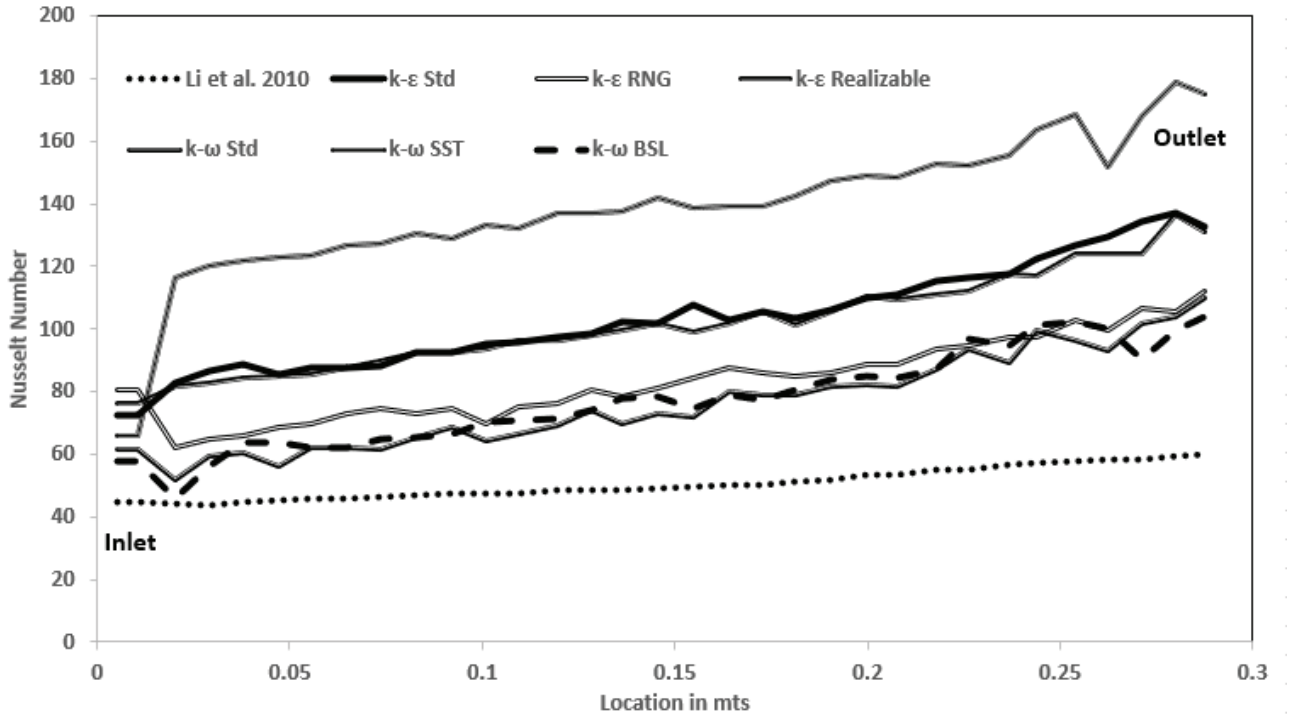

Figure 7. Local Nusselt Number variation along the pipe length. (Li et al. [11]: Downward Flow, P=8.80 MPa, T_{in} = 25^{0}C, Re_{in} = 9000.)

RESULTS AND DISCUSSIONS

With the validated Mesh model and the turbulence model, Wide ranges of mass flux, and heat flux cases are investigated in the present work. Based on the previous studies as shown in Table 2, the range of Heat flux and Mass flux values were considered in the present study. Mass flux is varied from 238 kg/m^{2}s to 1038 kg/m^{2}s (9 Cases), and heat flux from 26 kW/m^2 to 250 kW/m^2 (9 Cases).

Effect of Mass Flux

Figures 8, 9 and 10 show the effect of mass flux on the bulk fluid temperature, wall temperature and heat transfer coefficient respectively. As the mass flux increased outlet temperature of the bulk fluid decreased, also decreasing the wall temperature at higher mass values. This shows the clear improvement in heat transfer abilities at higher mass flux values. A peak in the wall temperature is observed at all the mass flux values for which pseudocritical temperature is achieved within the length of the pipe. At a high mass flux value of 638 kg/m^2-s (Case D), a peak in the wall temperature is not present for the entire length. Drastic decrease of heat transfer coefficient is observed at locations where the wall temperature peaks indicating the presence of hot spots resulting in heat transfer deterioration. Hence, it is desirable to use the higher mass flux values in a flow, such that the peak for the wall temperature doesn't occur at the entire length of the pipe and in turn, the issue of heat transfer deterioration will not be present (Case D). A total of 9 different mass flux cases ranging from 238 kg/m^2-s to 1038 kg/

Table 2. Range of Parameters considered in the literature for experimental and numerical studies

Reference Paper	Pressure (bar)	Heat Flux (kW/m^2)	Mass Flux (kg/m^2-s)	Flow Orientation
Hall and Jackson [2]	75.8	40–57	$Re_{in} = 113\times10^3$	Vertical
Tanaka et al. [3]	81	488; 640	120–240	Vertical
Petukhov et al. [17]	98	85–505	960	Vertical
Miropol'skiy and Baigulov [18]	79	67–224	670–770	Vertical
P.J Bourke et al. [4]	74.4–103.2	8–350	310-1700	Vertical
Bae et al. [8]	77.5 and 81.2	30–170	285–1200	Vertical
Kim et al. [15]	74.6 to 102.6	38 to 234	208 to 874	Vertical

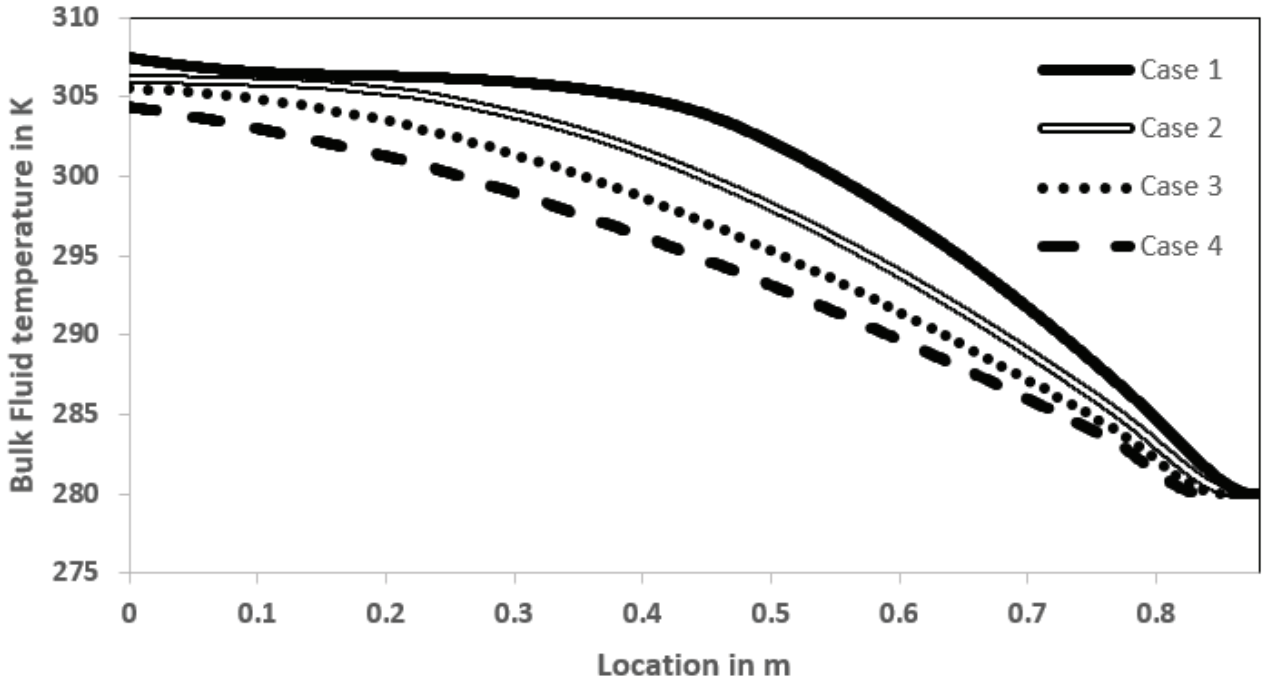

Figure 8. Variation of Bulk fluid temperature along the pipe length for different mass flux cases. Case 1: q"=52000kW/m^2, G=338 kg/m^2-s, P=7.621 MPa; Case 2: q"=52000kW/m^2, G=438 kg/m^2-s, P=7.621 MPa; Case 3: q"=52000kW/m^2, G=538 kg/m^2-s, P=7.621 MPa; Case 4: q"=52000kW/m^2, G=638 kg/m^2-s, P=7.621 MPa.

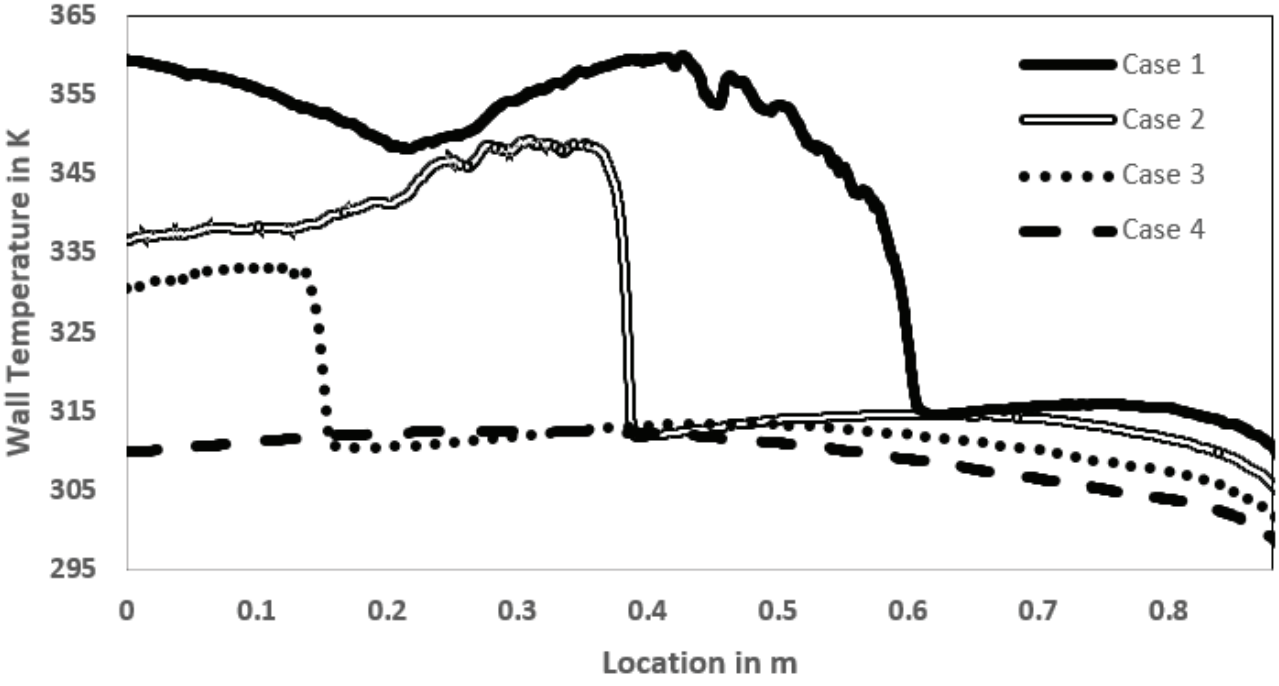

Figure 9. Variation of wall temperature along the pipe length for different mass flux cases. Case 1: q"=52000kW/m^2, G=338 kg/m^2-s, P=7.621 MPa; Case 2: q"=52000kW/m^2, G=438 kg/m^2-s, P=7.621 MPa; Case 3: q"=52000kW/m^2, G=538 kg/m^2-s, P=7.621 MPa; Case 4: q"=52000kW/m^2, G=638 kg/m^2-s, P=7.621 MPa.

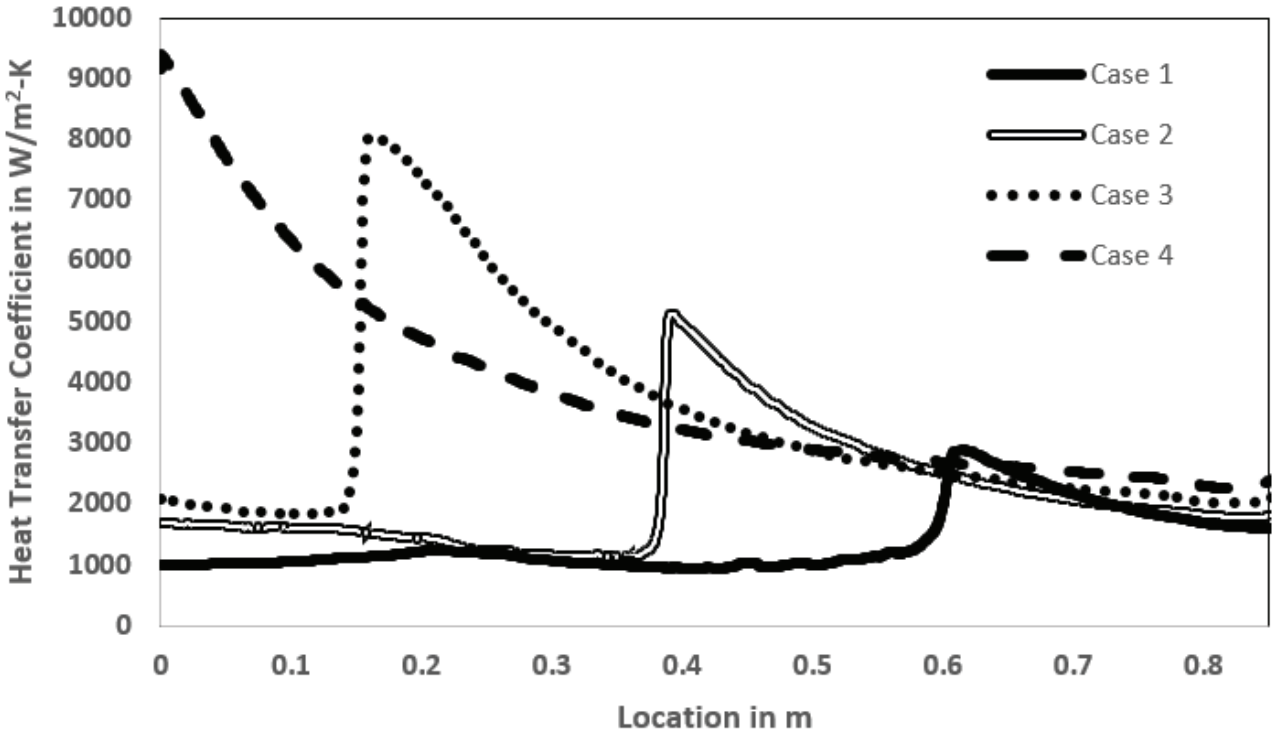

Figure 10. Variation of Heat Transfer Coefficient along the pipe length for different mass flux cases. Case 1: q"=52000kW/m², G=338 kg/m²-s, P=7.621 MPa; Case 2: q"=52000kW/m², G=438 kg/m²-s, P=7.621 MPa; Case 3: q"=52000kW/m², G=538 kg/m²-s, P=7.621 MPa; Case 4: q"=52000kW/m², G=638 kg/m²-s, P=7.621 MPa.

m²-s are considered to collect large data sets for Artificial neural network (ANN) studies.

Effect of Heat Flux

Figures 11,12 and 13 show, the variation of bulk fluid temperature, wall temperature and heat transfer coefficient for different heat flux boundary conditions respectively. An increase in the wall heat flux resulted in higher bulk fluid temperatures at the exit, also a spike in the bulk fluid temperature is observed at higher heat flux values. This spike is present for both bulk fluid temperature and wall temperature at higher heat flux values of greater than 200 kW/m². Peaks in the wall temperature are predominant compared to the peaks in Figure 12 shows the variation of heat transfer coefficient for different heat flux conditions, where there is a sudden decrease in heat transfer coefficient values at higher heat flux values and also this drop is followed by a recovery phase where the heat transfer coefficient will reach to its higher values. While this recovery phase was not present at different mass flux conditions. A total of 9 different heat flux cases ranging from 26 kW/m² to 250 kW/m² is considered to collect large data sets for Artificial neural network (ANN) studies.

Figure 14, shows the variation of the temperature difference between bulk fluid and wall along the length of the pipe and also the heat transfer coefficient. It is observed that the deterioration in heat transfer coefficient is due to the increase in temperature difference between the wall and the bulk fluid, this happens due to the sudden decrease in Cp values after the pseudo-critical point. As the temperature difference decreases, a recovery in heat transfer coefficient is observed irrespective of the heat flux values. The higher the wall heat flux, the greater the temperature difference and the lower the heat transferability. Hence it is desirable to use, higher values of mass flux for the cases where the heat flux values are very high.

Development of Ann Model

Artificial Neural Network (ANN) has been an indispensable tool in finding highly accurate correlations between independent variables and dependent variables inflow & thermal problems. This method comes under the broad umbrella of deep learning. ANN is a supervised learning technique, that requires the dataset to comprise both the independent and dependent variables. The neural network learns any non-linear relationship based on the supplied data. Once it has learnt the underlying relationship, it is possible to predict the dependent variable on the data which is unseen by the network.

In the present study, a correlation is proposed between Nusselt number (Nu) and independent variables such as Prandtl number (Pr), Reynolds number (Re), Grashoff number based on heat flux (Gr_q), non-dimensional heat flux

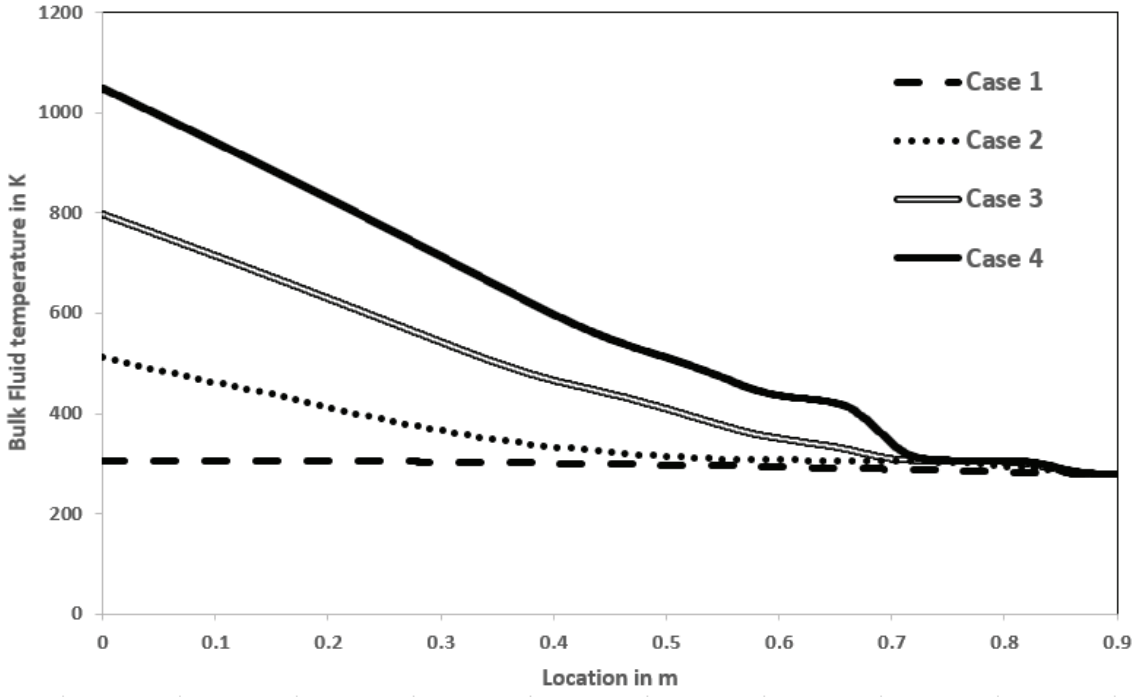

Figure 11. Variation of Bulk fluid temperature along the pipe length for different heat flux cases. Case 1: q"=26 kW/m^2, G=238 kg/m^2-s, P=7.621 MPa; Case 2: q"=104 kW/m^2, G=238 kg/m^2-s, P=7.621 MPa; Case 3: q"=182 kW/m^2, G=238 kg/m^2-s, P=7.621 MPa; Case 4: q"=250 kW/m^2, G=238 kg/m^2-s, P=7.621 MPa.

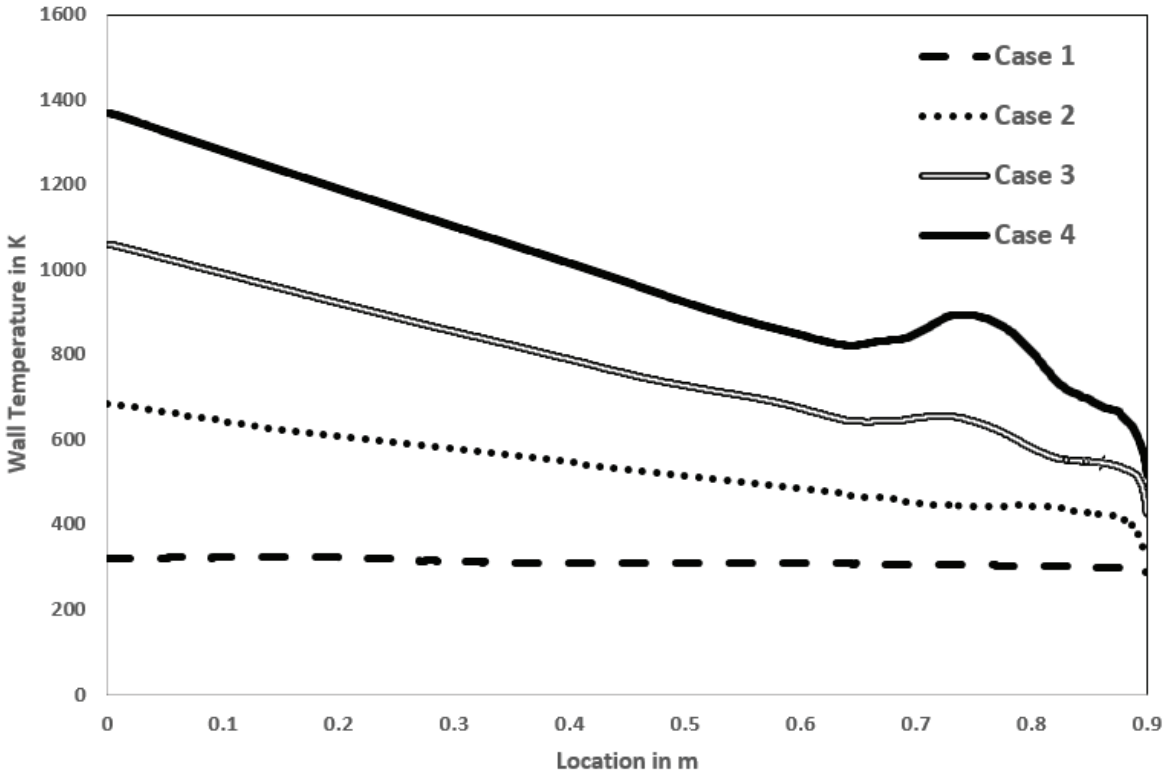

Figure 12. Variation of wall temperature along the pipe length for different heat flux cases. Case 1: q"=26 kW/m^2, G=238 kg/m^2-s, P=7.621 MPa; Case 2: q"=104 kW/m^2, G=238 kg/m^2-s, P=7.621 MPa; Case 3: q"=182 kW/m^2, G=238 kg/m^2-s, P=7.621 MPa; Case 4: q"=250 kW/m^2, G=238 kg/m^2-s, P=7.621 MPa.

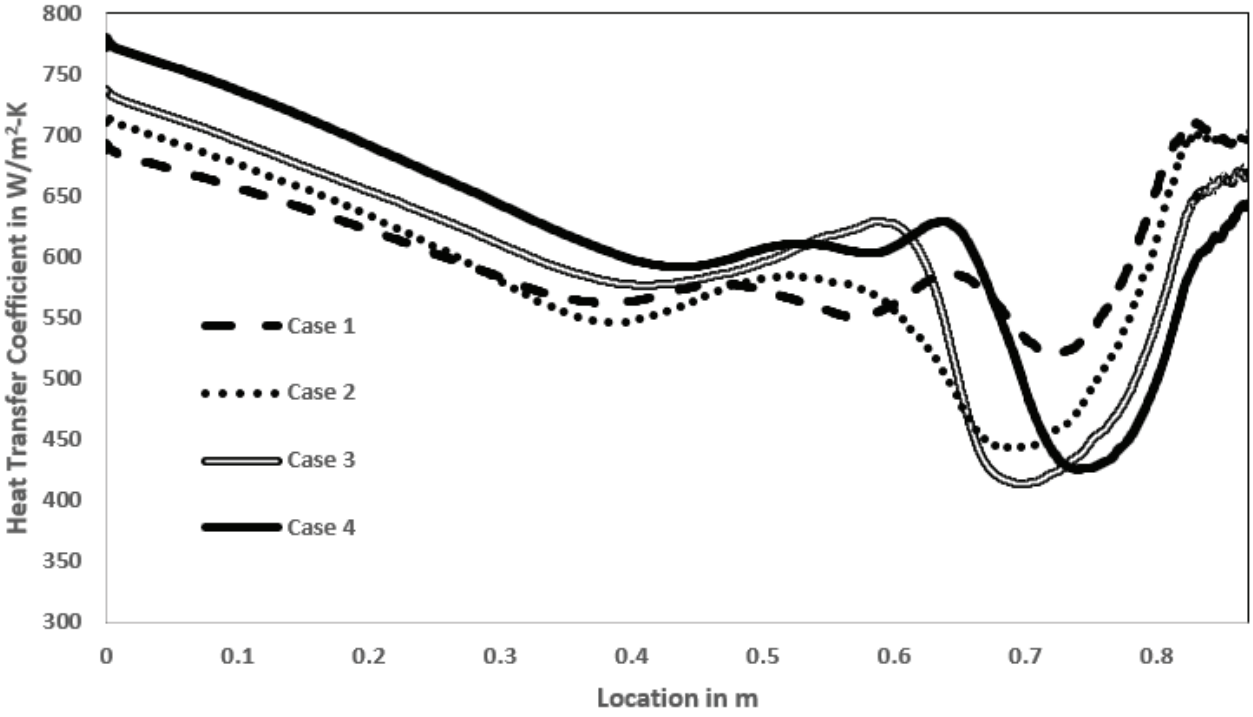

Figure 13. Variation of Heat Transfer Coefficient along the pipe length for different heat flux cases. Case 1: q"=26 kW/m^2, G=238 kg/m^2-s, P=7.621 MPa; Case 2: q"=104 kW/m^2, G=238 kg/m^2-s, P=7.621 MPa; Case 3: q"=182 kW/m^2, G=238 kg/m^2-s, P=7.621 MPa; Case 4: q"=250 kW/m^2, G=238 kg/m^2-s, P=7.621 MPa.

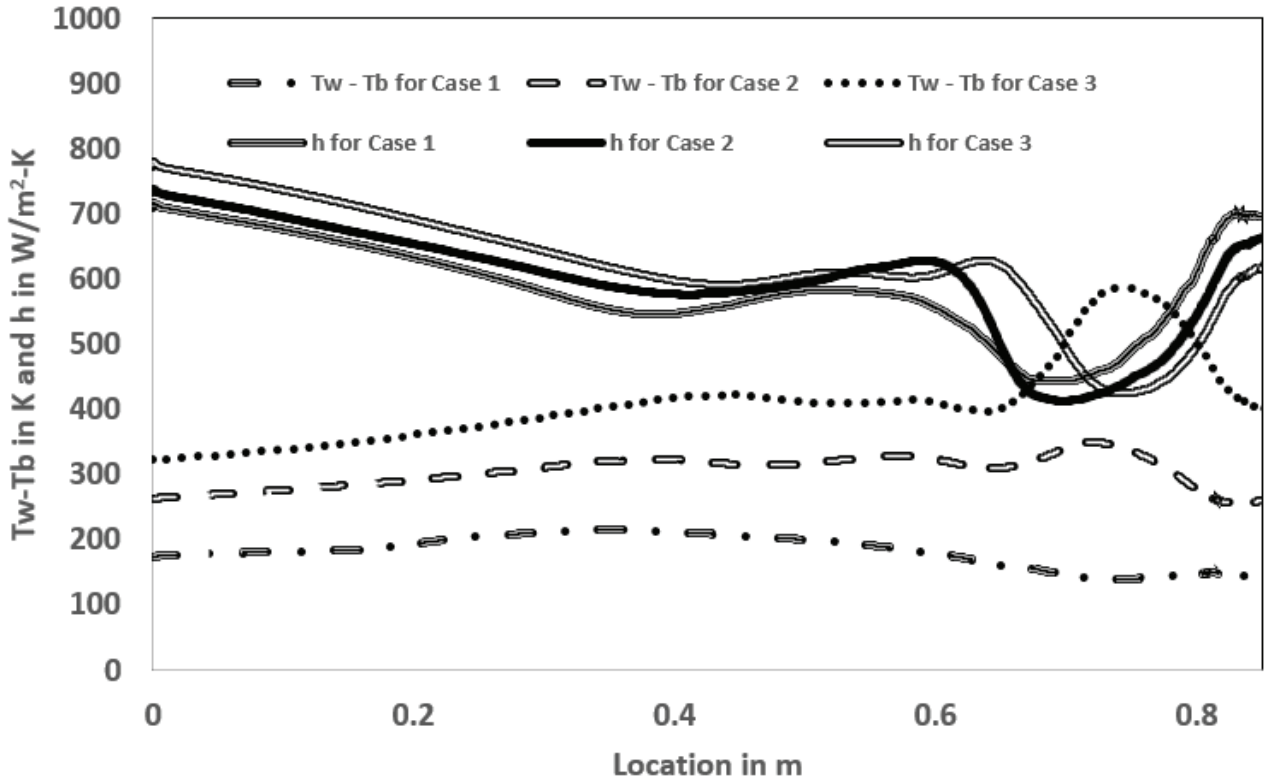

Figure 14. Variation of Heat Transfer Coefficient and Temperature difference between wall and the Bulk Fluid (Tw-Tb), along the pipe length for different heat flux cases. Case 1: q"=104 kW/m^2, G=238 kg/m^2-s, P=7.621 MPa; Case 2: q"=182 kW/m^2, G=238 kg/m^2-s, P=7.621 MPa; Case 3: q"=250 kW/m^2, G=238 kg/m^2-s, P=7.621 MPa.

(q^+) for the downward flow of supercritical carbon dioxide in a circular tube. This task has been achieved by scripting in Python language using the library called TensorFlow version 2.6.0. The code is executed on Google's cloud computing platform known as Collaboratory. A vast dataset consisting of 81414 samples obtained from CFD simulations is used to train the network. This data repository is prepared by calculating the above variables along the axis of the tube under variable mass flux and variable heat flux conditions. The whole dataset is split into training and testing sets in the ratio of 7:3. Subsequently, the testing set is further split into testing and validation sets in the ratio of 8:2. This distribution is necessary to make sure that the trained model performs with the same accuracy on unseen data too.

The neural network learns the relationship between the dependent variable and the independent variables by iteratively updating the model parameters (weights & biases) based on the backpropagation algorithm. According to this algorithm, the model learns the mapping function i.e., the model parameters by minimizing the loss function. It is very common to use Mean Squared Error (MSE) as the loss function and the same is used in the present study also. The MSE loss is given by equation (4).

$$MSE = \frac{1}{N}\sum_{i=1}^{N}\left(y_{pred} - y_{act}\right)^2 \quad (4)$$

The ANN developed here has four inputs and a single output as shown in Figure 15. The most important hyperparameters in ANN modelling are the number of hidden layers, number of neurons in each hidden layer, loss function optimization algorithm and the learning rate. An increase in the number of hidden layers helps to capture low-level input features influencing the output. While increasing the number of neurons helps in capturing highly non-linear relationships. Increasing the number of hidden layers and the number of neurons leads to the utilization of higher computational resources like memory and time since the number of parameters to be learnt by the ANN model is increased. A deep neural network architecture having 4 hidden layers and 15 neurons in each hidden layer was the best model based on several experiments as listed in Table 4 and the corresponding results are tabulated. ReLU (Rectified Linear Unit) activation function is applied to the output of each neuron in all the hidden layers and a linear activation function is applied to the neurons in the output layer. This model gave an R^2 score of 0.997 on the training set and 0.996 on the test set. The overall training time for this model was about 9 minutes. The complete details of the model are presented in Table 4.

Table 3. ANN model details

Input parameters	Pr, Re, Gr_q, q^+
Output parameter	Nu
Number of hidden layers	4
Number of neurons per layer	15
Activation function	ReLU
Optimization algorithm	Adam
Number of data samples	81414
Learning rate	0.001
Total number of weights & bias	811

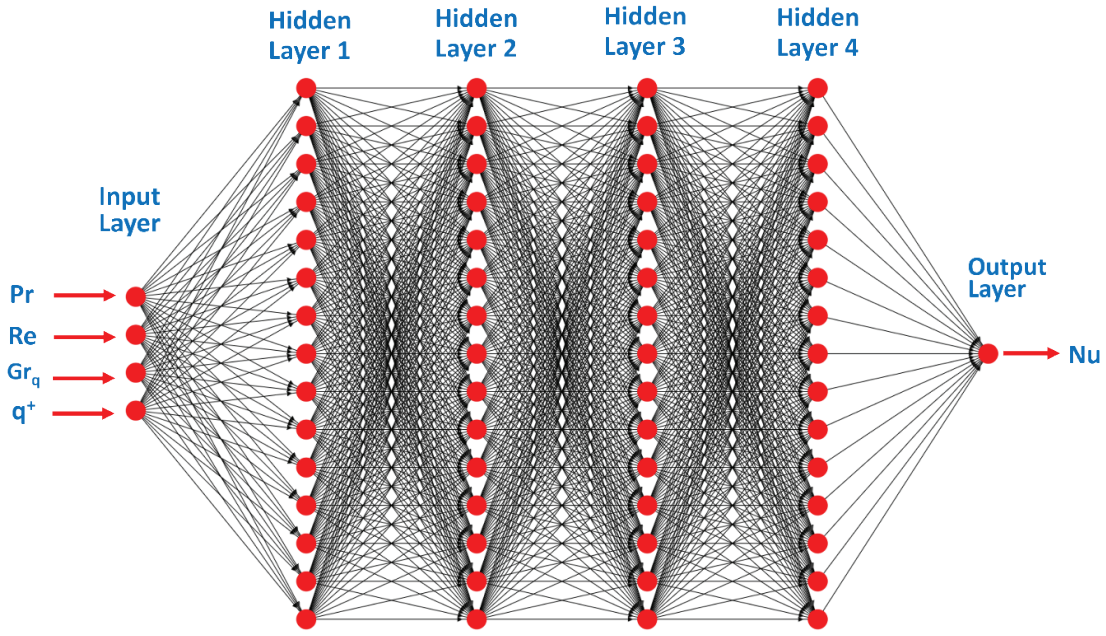

Figure 15. A rendering of the ANN used in the development of the Nusselt number correlation.

Table 4. Performance metrics monitored during hyperparameter tuning

Model Assessment Parameters	Number of neurons in each of the 4 hidden layers				
	10	**15**	**20**	**25**	**30**
R^2 score of training dataset	0.996	0.998	0.998	0.997	0.998
R^2 score of testing dataset	0.985	0.996	0.997	0.989	0.998
AARD%	3.885	2.183	1.967	1.847	1.495
Max AARD%	52.685	63.266	51.658	60.942	53.17
% of data samples with error < 5%	83.436	97.226	97.054	96.111	98.483
% of data samples with error > 5% & < 10%	14.441	2.050	2.395	2.486	1.179
% of data samples with error > 10%	2.122	0.723	0.550	1.402	0.337

Figure 16 shows the graph between the Nusselt number predicted by ANN and the Nusselt number obtained from flow simulation using Ansys Fluent. 97.226 % of the data samples lie within the error band of +/-5% and 2.050 % of the data samples lie between the error band of +/- 5 % and +/- 10%. The Absolute Average Relative Deviation (AARD %) is equal to 2.183 %.

$$AARD\ \% = \frac{1}{N}\sum_{i=1}^{N}\left|\frac{y_{pred}-y_{act}}{y_{act}}\right| \tag{6}$$

Mathematically, the ReLU function is defined as,

$$f(x) = (0,x)\ = \{\ 0,\ x \le 0;\ x,\ x > 0 \tag{7}$$

Figure 17 illustrates the decay of the MSE loss function over the number of training epochs (epoch is the number of times that all the data has been cycled through). The model converged at a training loss of 15.813 and a validation loss of 10.256. It is evident from the graph that the model is not exhibiting the commonly faced problems in ANN modelling such as overfitting or underfitting since the training and validation curves are overlapping each other.

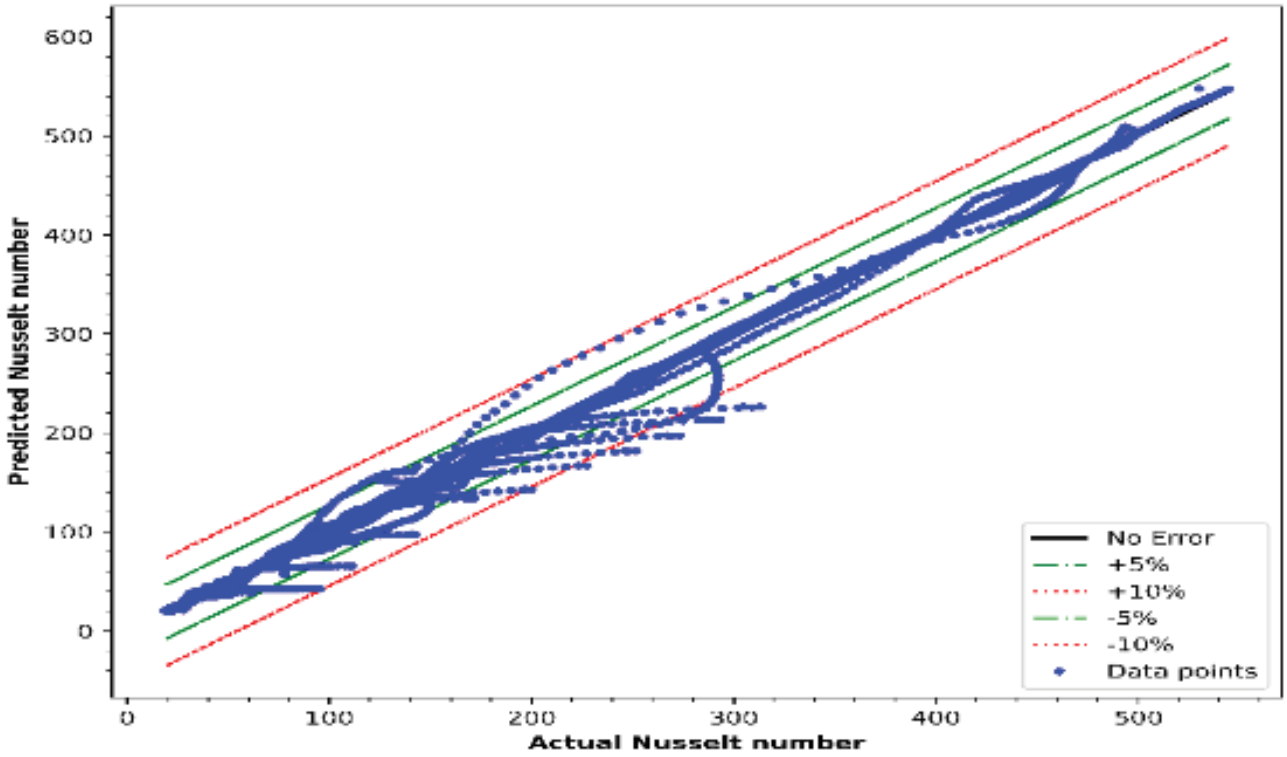

Figure 16. The graph showing the percentage deviation.

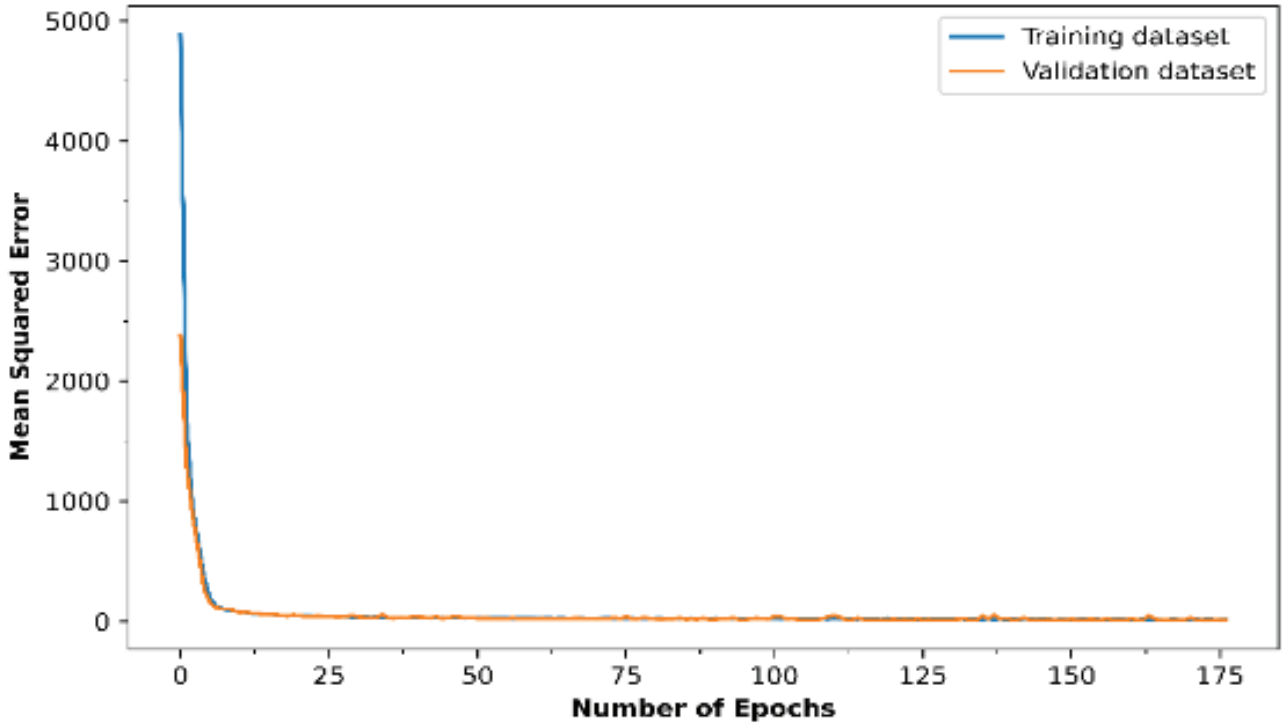

Figure 17. Learning curves.

Table 5. Description of model parameters

Symbol	Description	Matrix Shape
y	Output vector of ANN model, Nusselt Number (Nu)	1 x 1
X	Input vector to the ANN model, [Pr, Re, Gr_q, q^+]	1 x 5
b_1	Bias vector for the 1st hidden layer	15 x 1
b_2	Bias vector for the 2nd hidden layer	15 x 1
b_3	Bias vector for the 3rd hidden layer	15 x 1
b_4	Bias vector for the 4th hidden layer	15 x 1
b_o	Bias vector for the output layer	1 x 1
W_{i-1}	Weight matrix between the input layer and 1st hidden layer	5 x 15
W_{1-2}	Weight matrix between the 1st and 2nd hidden layer	15 x 15
W_{2-3}	Weight matrix between the 2nd and 3rd hidden layer	15 x 15
W_{3-4}	Weight matrix between the 3rd and 4th hidden layer	15 x 15
W_{4-o}	Weight matrix between the 4th hidden layer and output layer	15 x 1

To illustrate the prediction performance of the ANN model developed in the present study, the variation of the output variable (Nusselt number of supercritical CO_2) with the pipe location is graphically represented in Figure 18, for the constant mass flux of 238 kg/m^{2}s and a heat flux of 250 kW/m^2. The Nusselt number predicted by ANN closely follows the Nusselt number given by CFD simulations. Figure 19 shows the Performance comparison between ANN, CFD and Experimental Values. Near the pseudocritical region, due to the sudden increase in the thermal conductivity value, CFD results show a large increase in Nusselt Number values for small length. Except for the small region, CFD results, ANN Predictions and experimental results agree well. This indicates that the model is now ready to be tested on unseen data.

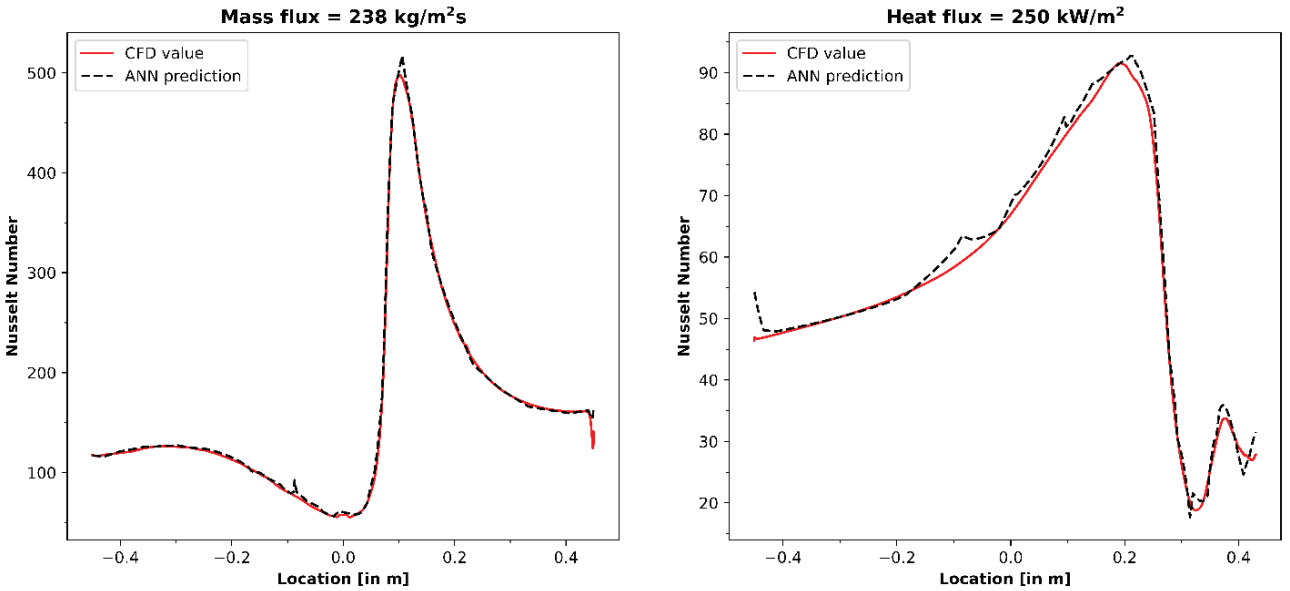

Figure 18. Performance comparison between ANN model and CFD model.

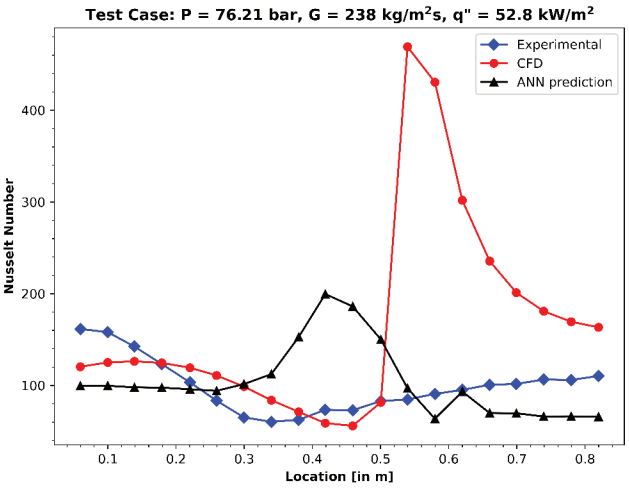

Figure 19. Performance comparison between ANN, CFD and Experimental Values.

CONCLUSION

Heat transfer characteristics of the vertically downward flow of supercritical carbon dioxide in a pipe are validated using the commercially available software ANSYS Fluent. The k-ω STD model with enhanced wall treatment along with third-order discretization for density, momentum, turbulent kinetic energy, turbulent dissipation rate and energy terms is found to give better accuracy in calculating bulk fluid temperature and wall temperature. The average error % in the bulk fluid temperature and the wall temperature is 1% and 2% respectively.

Parametric studies for the mass flux (238 kg/m²s to 1038 kg/m²s) and heat flux (26 kW/m² to 250 kW/m²) shows that, increasing the mass flux at a given heat flux at the wall would result in a smaller peak of wall temperature resulting in fewer chances of the presence of hot spots, A very large dataset consisting of 81,432 samples under varied operating conditions such as mass flux, and heat flux, are considered in the development of the ANN model to predict the heat transfer coefficient. A deep neural network architecture consisting of 4 hidden layers and 15 neurons in each layer was judged to be the generalized model after trying multiple architectures and comparing their goodness of fit. This model has an R^2 score of 0.998 and an AARD of 2.183%. The Authors strongly recommend the use of these ANN models to predict the heat transfer coefficient in the range of operating conditions prescribed in the studies.

NOMENCLATURE

C_p	Specific heat, kJ kg^{-1}
D	Pipe diameter, m
T	Temperature in K
u	Fluid velocity in m/s
G	Mass flux, kg m^{-2} s^{-1}
τ	Shear Stress in N/m^2
g	Acceleration due to gravity, m s^{-2}
Gr_q	Grashoff number based on heat flux, $g\beta D^4 q\rho^2/\mu^2 k$
h	Heat transfer coefficient, W m^{-2} K^{-1}
k	Thermal conductivity, W m^{-1} K^{-1}
N	Total number of samples in the training dataset
Nu	Nusselt number, hD/k
P	Pressure, Pa
P*	Critical pressure of CO_2, Pa

Pr Prandtl number
q Heat flux, Wm^{-2}
q^+ Acceleration parameter, $q\beta/GC_p$
Re Reynolds number
y_{act} Output variable obtained from CFD simulation
y_{pred} Output variable prediction of ANN model

Greek Symbols
β Thermal expansion coefficient, K^{-1}
μ Dynamic viscosity, kg m^{-1} s^{-1}
ρ Density, kg m^{-3}

Subscripts/ Superscripts
i,j,k Direction Cosines

AUTHORSHIP CONTRIBUTIONS

Authors equally contributed to this work.

DATA AVAILABILITY STATEMENT

The authors confirm that the data that supports the findings of this study are available within the article. Raw data that support the finding of this study are available from the corresponding author, upon reasonable request.

CONFLICT OF INTEREST

The author declared no potential conflicts of interest with respect to the research, authorship, and/or publication of this article.

ETHICS

There are no ethical issues with the publication of this manuscript.

REFERENCES

[1] Kruizenga A, Anderson M, Fatima R, Corradini M, Towne A, Ranjan D. Heat transfer of supercritical carbon dioxide in printed circuit heat exchanger geometries. J Therm Sci Eng Appl 2011;3:031002. [CrossRef]
[2] Hall WB. Heat transfer near the critical point. Adv Heat Transf 1971;7:1−86. [CrossRef]
[3] Hiroaki T, Nishiwaki N, Hirata M, Tsuge A. Forced convection heat transfer to fluid near critical point flowing in circular tube. Int J Heat Mass Transfer 1971;14:739−750. [CrossRef]
[4] Bourke PJ, Pulling DJ, Gill LE, Denton WH. Forced convective heat transfer to turbulent CO2 in the supercritical region. Int J Heat Mass Transfer 1970;13:1339−1348. [CrossRef]
[5] Fang X. Modeling and analysis of gas coolers. Air Conditioning and Refrigeration Center. College of Engineering. University of Illinois at Urbana-Champaign; 1999.
[6] Duffey RB, Pioro IL. Experimental heat transfer of supercritical carbon dioxide flowing inside channels (survey). Nucl Eng Des 2005;235:913−924. [CrossRef]
[7] Jiang P, Zhao C, Deng J, Zhang W. Experimental investigation of local heat transfer of carbon dioxide at super-critical pressures in a vertical tube and multi-port mini-channels under cooling conditions. International Refrigeration and Air Conditioning Conference, Purdue University, 2008.
[8] Bae YY, Kim HY, Kang DJ. Forced and mixed convection heat transfer to supercritical CO2 vertically flowing in a uniformly-heated circular tube. Exp Therm Fluid Sci 2010;34:1295−1308. [CrossRef]
[9] Zhang Y, Zhang C, Jiang J. Numerical simulation of heat transfer of supercritical fluids in circular tubes using different turbulence models. J Nucl Sci Technol 2011;48:366−373. [CrossRef]
[10] Fang X, Xu Y. Modified heat transfer equation for in-tube supercritical CO2 cooling. Appl Therm Eng 2011;31:3036−3042. [CrossRef]
[11] Ye K, Zhang Y, Yang L, Zhao Y, Li N, Xie C. Modeling convective heat transfer of supercritical carbon dioxide using an artificial neural network. Appl Therm Eng 2019;150:686−695. [CrossRef]
[12] Wang J, Guo P, Yan J, Zhu F, Luo X. Experimental study on forced convective heat transfer of supercritical carbon dioxide in a horizontal circular tube under high heat flux and low mass flux conditions. Adv Mech Eng 2019;11:1687814019830804. [CrossRef]
[13] Liao SM, Zhao TS. Measurements of heat transfer coefficients from supercritical carbon dioxide flowing in horizontal mini/micro channels. J Heat Transfer 2002;124:413−420. [CrossRef]
[14] Rajendra Prasad KS, Krishna V, Sachin Bharadwaj M, Ponangi BR. Turbulent heat transfer characteristics of supercritical carbon dioxide for a vertically upward flow in a pipe using computational fluid dynamics and artificial neural network. J Heat Transfer 2022;144:011802. [CrossRef]
[15] Kim DE, Kim MH. Experimental study of the effects of flow acceleration and buoyancy on heat transfer in a supercritical fluid flow in a circular tube. Nucl Eng Design 2010;240:3336−3349. [CrossRef]
[16] Li Z-H, Jiang P-X, Zhao C-R, Zhang Y. Experimental investigation of convection heat transfer of CO2 at supercritical pressures in a vertical circular tube. Exp Therm Fluid Sci 2010;34:1162−1171. [CrossRef]
[17] Petukhov BS. Heat transfer and friction in turbulent pipe flow with variable physical properties. Adv Heat Transf 1970;6:503−564. [CrossRef]
[18] Miropolsky ZL, Baigulov VI. Investigation in heat transfer, velocity and temperature profiles with carbon dioxide flow in a tube over the nearly critical region of parameters. Int Heat Transfe Conference Digital Library. New York: Begel House Inc.; 1974. [CrossRef]